ELSEVIER

Polymer 41 (2000) 8869–8878

polymer

www.elsevier.nl/locate/polymer

High pressure differential scanning calorimetry of poly(4-methyl-pentene-1)

G.W.H. Höhne[a,*], S. Rastogi[b], B. Wunderlich[1,c,d]

[a]*Section Calorimetry, University of Ulm, P.O. Box 4066, 89069 Ulm, Germany*
[b]*Eindhoven Polymer Laboratories/The Dutch Polymer Institute, Eindhoven University of Technologie, P.O. Box 513, 5600 MB Eindhoven, The Netherlands*
[c]*Department of Chemistry, The University of Tennessee, Knoxville, TN 37996-1600, USA*
[d]*The Chemical and Analytical Sciences Division, Oak Ridge National Laboratory, Oak Ridge, TN, USA*

Received 5 August 1999; received in revised form 8 February 2000; accepted 8 February 2000

Abstract

The polymer poly(4-methyl pentene-1), P4MP1, displays an unusual pressure–temperature phase diagram. The previous exploration of this phase behavior through X-ray diffraction has been extended through high-pressure calorimetry. The resulting phase diagram displays a melt area, the common tetragonal crystal phase, and a high-pressure phase of hexagonal symmetry. Below the glass transition temperature of the amorphous fraction, the tetragonal phase can be disordered by application of pressure in what seems to be a frustrated transition that leads to a conformationally disordered glass. The transitions between the phases, previously postulated on structural evidence, are supported by calorimetry. Observed are the following: (1) isothermal crystal disordering by increasing of pressure; (2) isobaric crystal perfection on heating, and disordering on cooling; (3) sign inversion of the pressure coefficient of the melting temperature. Equilibrium and nonequilibrium features of the phase diagram are discussed. © 2000 Elsevier Science Ltd. All rights reserved.

Keywords: High-pressure calorimetry; Poly(4-methyl pentene-1); Phase diagram

1. Introduction

Poly(4-methyl pentene-1) (P4MP1) is a semicrystalline polymer with a stable, tetragonal symmetry at atmospheric pressure. Within the tetragonal crystals two helical chains of type $2^*7/2$ make up the unit cell. In the helix, seven of the two-chain-atom repeating-units go through two turns per helix repeat [1]. A low packing fraction of 0.57 at room temperature, and a melting temperature, T_m, of about 245°C at atmospheric pressure characterize the crystals. The amorphous phase at room temperature, in contrast, has a packing fraction of 0.59. The respective packing-fractions of polyethylene are 0.70 and 0.60. This clearly illustrates the open packing of the P4MP1 crystal and its similar packing in the melt. The higher melting temperature than for polyethylene (141.4°C) results from the added enthalpy of fusion at similar entropy of fusion per chain atom. The glass of P4MP1 has a transition temperature, T_g, in the range of 45–50°C, compared to −36°C of polyethylene, and indicative of less mobile chains. This also means, however, that below T_g the calculated crystal density is lower than the amorphous density. Somewhat above T_g, the higher density of crystal versus melt is reestablished. On application of pressure below the glass transition temperature it was observed by in situ X-ray diffraction and Raman spectroscopy that the long range, crystalline order in the tetragonal phase is lost [2–4]. This research result was interpreted as a "solid state amorphization." Such a phenomenon of amorphization on application of pressure has also been found for ice when compressed below the glass transition temperature of about −130°C [5,6]. Ice and P4MP1 have a similar density relationship, so that the drive to decrease the density with pressure may be taken as the reason for the loss of order on compression. The difference between the two materials is that ice consists of motifs of small molecules which need only limited large-amplitude motion (rotation and translation) to disorder, while P4MP1 as a flexible macromolecule can only disorder by conformational motion (internal rotation). Below the glass transition, however, the macromolecules should not be able to undergo the major reorganization necessary to become the random coils of the amorphous phase. After the "solid-state amorphization," the chains of P4MP1 are, indeed, still largely parallel [4], i.e. P4MP1

* Corresponding author. Tel.: +1-423-974-0652; fax: +1-423-974-3419.

E-mail address: athas@utk.edu (G.W.H. Höhne).

[1] The submitted manuscript has been authored by a contractor of the US Government under the contract no. DE-ACO5-960R22464. Accordingly, the US Government retains a nonexclusive, royalty-free license to publish, or reproduce the published form this contribution, or allow others to do so, for US Government purposes.

0032-3861/00/$ - see front matter © 2000 Elsevier Science Ltd. All rights reserved.
PII: S0032-3861(00)00230-5

assumes a state that may be classified as a glass with a condis crystal structure, also called a CD glass [7].

Since on heating the crystals of P4MP1 become denser than the liquid, the melting temperature increases with pressure, obeying the common form of the Clausius–Clapeyron equation ($dT_m/dp = \Delta V_f/\Delta S_f$) [8]. Increasing the pressure beyond 2 kbar (0.2 GPa), a maximum develops in the melting temperature, suggesting that there is not only an inversion of the density relationship with decreasing temperature, but also one with increasing pressures [2–4,9]. For ice, in contrast, the melting temperature decreases already by increasing the pressure beyond atmospheric conditions. This inversion of the liquidus line in the phase diagram of P4MP1 is rather unique. The inversion in the melting temperature with pressure at high temperature and the existence of a disordered state at low temperature at elevated pressure suggests a possible re-entry of the widely separated "liquid phase" (above the melting temperature) to the "solid-state amorphous phase" (below the glass-transition temperature) at high pressure [2–4].

The entry anticipated from the high-temperature liquid to the low-temperature amorphous phase or vice versa without crystallization, is prevented by the intervention of a new, crystalline high-pressure phase, with hexagonal symmetry and $2^*3/1$ helical chains [2–4]. As most other vinyl polymers with $2^*3/1$ helices, the unit cell of the new polymorph will most likely belong to the trigonal R3 space groups. The density of the hexagonal phase is higher than that of the tetragonal phase, as can be judged from the slope of the Clausius–Capeyron equation, as is seen in Fig. 7, below.

To gain insight into the nature of the phase transitions in this rather unusual macromolecule, a detailed thermodynamic study is needed. In this paper, we will report our experimental findings by high-pressure differential scanning calorimetry and discuss the nature of the phase transitions.

2. Experimental

In the present work the p–T phase behavior of P4MP1 was investigated with the help of a high pressure differential scanning calorimeter (HP-DSC). The material of investigation was the homopolymer isotactic P4MP1 from an industrial source having a melting temperature of 245°C and a heat of fusion of about 40 J g^{-1} at atmospheric pressure (3.4 kJ mol^{-1}, 34% crystallinity). The molecular mass and polydispersity were $M_w = 250,000$ and $M_w/M_n = 4.0$, respectively. The calorimetric measurements were carried out on unoriented, melt crystallized samples.

A special high pressure measuring head was constructed for a commercial power-compensated differential scanning calorimeter (DSC-7, Perkin–Elmer Corp.). This measuring head contains two small furnaces as the normal DSC, but placed in an autoclave. The details of this construction have been published elsewhere [10]. The essentials are the following: for safety, instead of a gas, silicon oil of medium viscosity was used as pressure transmitting fluid. For better heat conductivity, the reference and sample furnaces were constructed of silver instead of platinum. They are placed inside narrow cylindrical boxes of glass/ceramics to avoid heat leaks due to excessive convection and conduction. The volumes of these boxes were adjusted separately so that they contained equal amounts of oil on the sample and reference sides. The symmetry of the arrangement was crucial to overcome problems arising from the need to equalize the higher heat losses than in the gas-environment of the atmospheric-pressure DSC. Due to extrinsic conditions, there is a larger noise and a poorer reproducibility of the base line in the pressure cell than with the standard measuring heads. Subtraction of runs with empty pans is required to reduce the curvature of the base line. Calculations of the heat capacity of the sample give, however, incorrect results since the mass of oil cannot be reproduced with the necessary precision when exchanging sample and empty pans. Nevertheless, the sensitivity, compared with that of the common measuring head, is quite acceptable.

The specifications of the HP-DSC are as follows:

- *Thermal noise.* 50–100 μW;
- *Precision of detection.* 3 mJ (i.e. ≈ 1 J g^{-1});
- *Heating and cooling rates.* 0.5–30 K min^{-1};
- *Range of temperature.* 25–350°C;
- *Range of pressure.* 0.1–500 MPa (1–5 kbar);
- *Repeatability of the baseline.* 2–3 mW.

The calibration of the temperature and heat-flow rate were done, as recommended, with indium and tin as calibration substances [11]. Unfortunately reliable literature values exist only for indium for the pressure dependence of heat and temperature of fusion [12]. The literature data for the fusion of tin are not as precise as the indium values [13].

We found the temperature corrections of the HP-DSC to depend on temperature as well as on pressure, thus, the nonlinear correction had to involve a calibration table with both variables. During measurements, a small indium sample of 0.3 mg was always present in the reference pan for an online check of the calibration. The uncertainty of the measured temperatures, corrected in this fashion, is 1–5 K, depending on temperature and pressure. The greatest part of the uncertainty comes from the unreliable values for tin at elevated pressure and temperature.

For the calibration of the heat-flow rate, the situation is similar, the calibration factor depends both, on pressure and temperature. The reason for this double dependency is the large heat conductivity of the pressure medium which causes a much larger pressure and temperature dependent heat-leak than for the standard measuring heads [14]. The power-compensation principle, however, keeps the calibration factor close to a constant value (5–25% at lower pressure, 1–10% at higher pressure). Nevertheless, the precision of the measured heats of transition for the polymers is not better than 10% because of the broadening of the melting region and an unavoidable curving of the baseline which

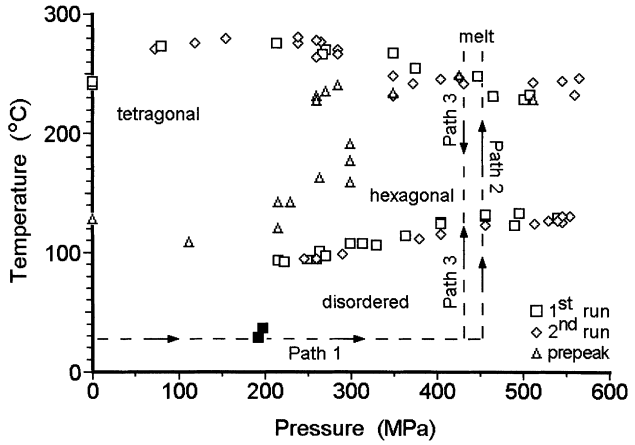

Fig. 1. Collection of all identified transition temperatures and schematic indication of the different analysis paths.

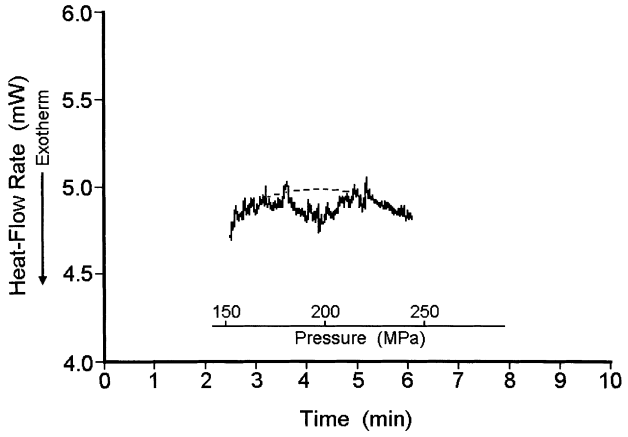

Fig. 3. Heat-flow rate trace at 300 K (27°C) for the disordering on a pressure rise of 20 MPa/min along path 1 of Fig. 1 (■ in Figs. 1 and 2).

leads to uncertainties in the integration (see for examples the Figs. 4 and 5, below).

All samples were hermetically sealed in aluminum pans to prevent any direct contact with the pressure medium (silicon oil). The encapsulation was done in a way avoiding cavities that would contain air and would lead to a deformed pan on increasing the hydrostatic pressure. The presented results are from six different samples with masses varying from 5 to 11 mg. The heating and cooling rates were 20 K min^{-1}, a rather fast rate, necessary because of the small transition effects which would otherwise not be detectable.

Three types of analyses for HP-DSC were carried out:

- a pressure-rise at constant, low temperature (isothermal path 1);
- a first increasing of temperature at constant pressure (isobaric path 2);
- subsequent isobaric runs (cooling and heating paths 3).

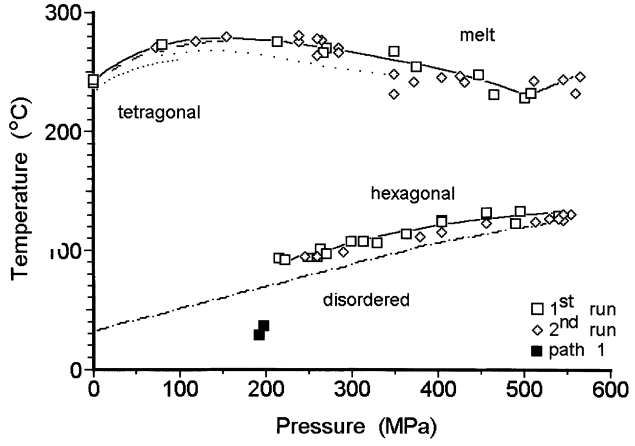

Fig. 2. Melting and transition temperatures as in Fig. 1 with drawn lines separating phase areas of different order, as detected by X-ray diffraction [2,3]. Omitted for clarity are the prepeaks identified in Fig. 1 as (△) and discussed below. The line marked ∼·∼ indicates the glass transition, derived from Brillouin scattering, the dashed line and dotted lines, melting data from the literature (see text).

Examples of the paths are included in Fig. 1.

The heat-flow rate curves obtained from runs along these pathways exhibit enthalpy peaks from different transitions which have been evaluated with respect to the peak temperature and the area between the measured curve and an interpolated baseline. After the necessary calibrations were carried out, the reported data represent the temperature of the maximum heat-flow rate at the given rate of heating or cooling and the corresponding enthalpies of transition.

3. Results

Fig. 1 represents a summary plot of all observed transition temperatures along the paths described above. The dashed lines mark examples of the isothermal and isobaric experiments. The transitions appear to scatter over the temperature–pressure plot. Removing the weak "prepeaks" (△) which could not be detected in every run, clarifies the graph, as shown in Fig. 2. The isothermal heat-flow rate of the HP-DSC run along path 1 gives at 30–40°C very weak, but reproducible, exothermic peaks in the pressure region of 200 MPa (■). A typical example is illustrated in Fig. 3.

A first isobaric heating along path 2 after the isothermal compression at low temperature yields clearly visible, endothermic melting peaks between 200 and 300°C (□ in Figs. 1 and 2). A typical example is illustrated by curve a of Fig. 4. At pressures above 200 MPa, the isobaric heating along path 2 yields an additional small endotherm at a much lower temperature which seems to belong to a solid–solid transition. An example is given by curve a in Fig. 5. These transitions appear again after cooling from the melt and reheating the sample at the same pressure (path 3, see Figs. 4 and 5, curves b). The endotherms on second heating occurred often at a somewhat lower temperature, as shown in curve b of Fig. 5 and are marked in Figs. 1 and 2 by (◇).

On isobaric cooling from the melt via path 3 there was a

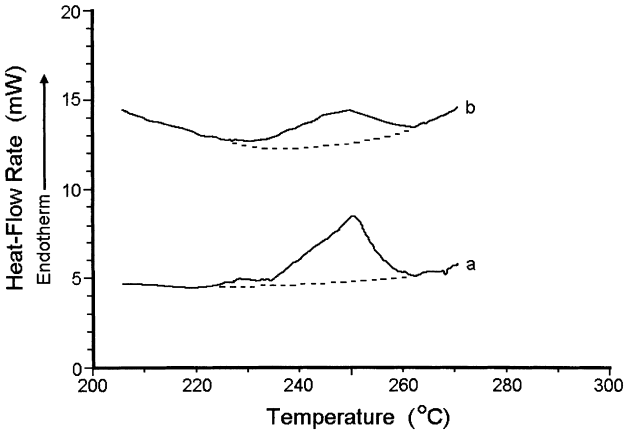

Fig. 4. Two examples of heat-flow rate traces at 550 MPa for the broad range of fusion shown in Fig. 2. Curve a, first heating (path 2, □). Curve b, second heating (path 3, ◇).

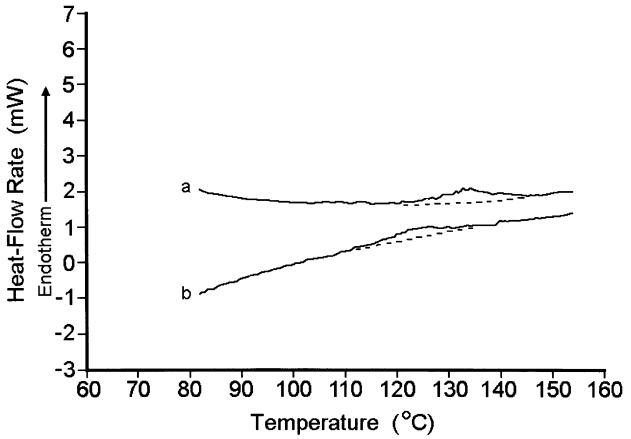

Fig. 5. Example heat-flow rate traces at 405 MPa for the small endotherms between 90 and 140°C in Fig.2. Curve a, first heating (path 2, □). Curve b, second heating (path 3, ◇).

large supercooling, as is common with macromolecules [15]. The crystallization temperature was always between 20 and 50 K lower than the corresponding melting temperature. Sometimes, there was even no visible crystallization endotherm. Reheating at the same pressure along path 3 leads to the same melting temperature as was obtained on the first heating via path 2. All measured fusion temperatures have been collected in Table 1.

Isobaric heating runs at different pressures via path 3 sometimes contain small endothermic peaks above 100°C (△ in Fig. 1) which we call prepeaks, as they appear at lower temperatures than the melting transition. These peaks could not be reproduced systematically, obviously their appearance depends on the thermal history of the sample, but in a presently unknown way.

The measured heats of transition are collected in Table 2. Besides the melting and crystallization, only very weak transitions exist, requiring measurements at the limit of resolution of the HP-DSC. The uncertainty of the measurements in terms of heat evolved or absorbed is ±10%, but the

Table 1
Measured transition temperatures of P4MP1 at different pressures

Fusion path 2[a]		Fusion path 3[b]		Transition path 2[a]		Transition path 3[b]		Prepeak path 3[b]	
p (MPa)	*T* (°C)	*p* (MPa)	*T* (°C)	*p* (MPa)	*T* (°C)	*p* (MPa)	*T* (°C)	*p* (MPa)	*T* (°C)
0.1	241	0.1	241	215	93	246	94	0.1	127
0.1	243	73	271	222	92	260	95	113	107
80	274	120	276	250	94	290	98	215	119
214	275	155	280	260	94	380	111	215	141
267	267	239	276	263	101	405	115	230	141
270	271	239	281	270	98	456	123	230	141
350	268	260	278	300	107	514	125	260	227
375	255	260	263	313	108	530	127	260	230
448	249	260	265	330	106	540	127	263	162
465	232	265	278	364	114	545	126	263	162
500	229	285	267	405	125	545	131	270	234
507	234	286	270	405	126	555	131	285	240
565	245	350	232	456	132	–	–	300	158
–	–	350	249	490	123	–	–	300	158
–	–	372	243	496	130	–	–	300	176
–	–	405	246	–	–	–	–	300	190
–	–	425	248	–	–	–	–	350	233
–	–	432	242	–	–	–	–	425	248
–	–	512	244	–	–	–	–	512	228
–	–	546	244	–	–	–	–	–	–
–	–	560	233	–	–	–	–	–	–
–	–	565	247	–	–	–	–	–	–
–	–	565	248	–	–	–	–	–	–

[a] Isobaric heating after isothermal pressurizing to p at room temperature along path 1.
[b] Isobaric heating after isobaric cooling from the melt (second heating, path 3).

Table 2
Heats of transition of P4MP1

Transition	Heat (J g^{-1})	Comment
Path 1 at 200 MPa	−0.5 and −1.0	Exothermic
Path 2 at ≈ 100°C	1–2	Endothermic, on heating only
Path 3 at ≈ 100°C	1–2	Endothermic, on heating only
Paths 2 and 3 at ≈ 250°C	5–40	Endothermic fusion of the tetragonal crystal phase
Path 3 on cooling at ≈ 200°C	−30 to −25	Supercooled, exothermic crystallization
Path 3 at 120–200°C	< 1	Endothermic prepeak on heating

experimental accuracy is at least ±0.3 J g^{-1}. The events are, thus, clearly visible (see Figs. 3–5).

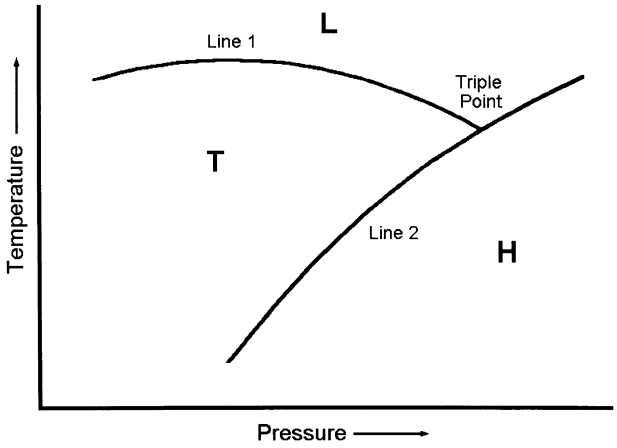

Fig. 6. Proposed schematic equilibrium phase-diagram for P4MP1.

4. Discussion

Before discussing the present research, it is expedient to clarify the terms disorder, amorphization, and phase diagram as used in this paper [1,16]. The term disorder is generally used in the description of the defect structure of crystals and denotes a deviation from crystalline order. More specifically, one distinguishes four categories of defects: (1) point defects; (2) dislocations or one-dimensional defects; (3) surfaces and grain boundaries; and (4) amorphous or three-dimensional defects [1]. The amorphous defects are in the two-phase model of semicrystalline polymers commonly called the "amorphous phase," but should be counted as crystal defects since their domains can be considered to be nanophases and are strongly coupled to the crystals by molecules that cross their boundaries. The amorphous defects are the cause of limited crystallinity, and as an indication of the strong interaction, one commonly finds in semicrystalline polymers an increased and broadened glass transition and sometimes even a rigid-amorphous fraction that shows no glass transition.

For flexible molecules the most common point defect is conformational disorder. This defect, when mobile, is linked to conformational, large-amplitude motion (internal rotation). Conformational disorder is produced by rotation about a flexible bond of the molecule to a different rotational isomer than is found in the ideal crystal structure. In small concentrations, point defects are present in most crystals, either as equilibrium or as nonequilibrium imperfections. They are at the root of the structure-sensitive properties [17]. Sometimes, crystals can cooperatively acquire a large equilibrium concentration of disorder, then the material is called a mesophase (intermediate between crystal and melt). Mesophases may have well-defined phase-transition temperatures to the liquid and crystal. The mesophase based on conformational disorder alone is called, for short, a condis crystal [7,18]. If the large-amplitude motion needed to maintain the dynamic equilibrium of creation and destruction of the defects is frozen at low temperature or high pressure, a glass results. In the case of condis crystals, this glass is called a CD glass. As all glasses, the CD glass is a solid, i.e. its internal energy is almost entirely based on its vibrational excitation.

A final comment concerns the term "phase diagram." Commonly it refers to the areas of existence of the various phases of a material and their boundaries, as governed by equilibrium thermodynamics. Semicrystalline polymers are never in equilibrium, best documented by the fact that they violate the phase rule. Equilibrium phase diagrams of polymers are thus rare, and most often obtained by extrapolation from data on nonequilibrium, semicrystalline polymers. Experience tells, however, that the nonequilibrium phase diagrams obtained by direct plotting of data gained from semicrystalline samples have largely parallel phase boundaries to the equilibrium diagram, although usually shifted by as much as 10–20°C. The nonequilibrium phase diagram is thus a good approximation to the expected equilibrium phase diagram.

4.1. Equilibrium phase diagram

The goal of any thermal analysis at varying temperatures and pressures should be the derivation of a phase diagram. From the data of Fig. 2 and with the indicated X-ray results [2–4], one can draw a schematic equilibrium phase diagram, as shown in Fig. 6. One expects the phase lines 1 and 2, as well as the triple point to be 10–20 K higher than suggested in Fig. 2, as discussed above. The main reason for the temperature shifts is the small crystal size, caused by the chain-folding principle obeyed by flexible, linear macromolecules [1]. The explanation for the parallel phase lines is the frequently identical heat capacities of different solid polymorphs ($d^2G/dT^2 = C_p/T$). No direct experimental information can be gained below the glass transition, also indicated in Fig. 2, but since it is possible to derive the contribution of the vibrational heat capacity using the methods derived from the ATHAS data bank [19], the diagram of Fig. 6 can be extended to lower temperatures and applied to

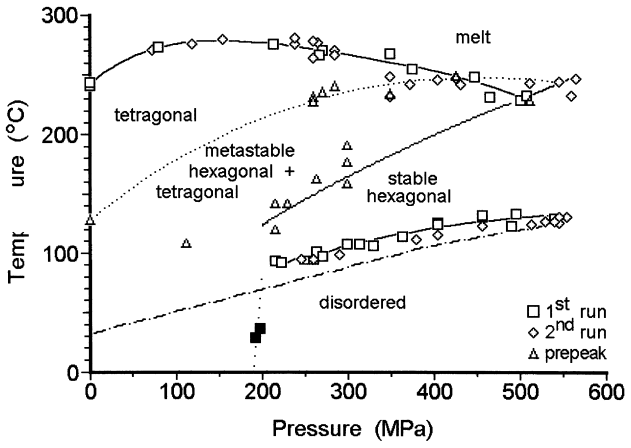

Fig. 7. Nonequilibrium phase diagram of P4MP1.

hypothetical equilibrium crystals which, naturally have no glass transition.

In the following sections of the paper all observed thermal effects will be used, together with literature data and information gained by other analysis techniques, to verify the schematic equilibrium phase diagram of Fig. 6. The different thermal observations will be discussed in sequence and lead, ultimately to the nonequilibrium phase diagram shown in Fig. 7 which summarizes the present knowledge about P4MP1. This phase diagram must be considered to refer to metastable states with arrested internal variables which describe the thermal and pressure history of the sample. The number, nature, and quantitative values of these internal variables are, as usual, not known. Commonly the thermal and pressure history is the only description available.

The close qualitative and quantitative resemblances between Fig. 7 and the phase diagram suggested by Rastogi et al. on the basis of X-ray diffraction data [2,3] are apparent and suggest that the measured DSC peaks correspond to the observed structural changes. Both show the same subdivision into phase regions within the p–T plane. The phase diagrams obtained by X-ray diffraction and by calorimetry can be regarded as practically identical, which we regard as one of the principal outcomes of this study.

4.2. Pressure-dependence of the melting temperature

The pressure dependence of the melting temperature of P4MP1 was of initial interest for the verification of the higher density of the crystals than the melt at the melting temperature [8]. The data were taken on a similar sample as used in the present research and are marked in Fig. 2 by the dashed line. They agree well with the present data, but were not carried to sufficiently high pressures to show a maximum. Two other sets of T_m vs. p data were generated using a P4MP1 with a somewhat lower melting point [9,20]. These data are represented by the dotted lines in Fig. 2. The overall lower melting temperature of these two data sets is mainly due to a larger copolymer content of the samples used. It also should be noted that our plotted values in the p–T diagram are the peak temperatures at a heating rate of 20 K min^{-1}. The melting peak, however, is rather broad (see Fig. 4) and superheating effects are possible, both allowing for variation in the data.

The melting curve in Fig. 2 shows an initial decrease in the slope from atmospheric pressure to 150 MPa, followed by an almost horizontal slope from 150 to 250 MPa, and then a negative slope above 250 MPa. Such a change of the slope to negative values is unusual. Most polymers show only a gradual decrease in dT_m/dp. To obtain a more precise accord between different measurements than shown in Fig. 2, a well-defined point of the broad melting curve must be chosen, free of instrument and sample history effects, and corrected for differences in purity of the sample (as expressed by tacticity, chemical purity, molar mass, etc.). The available data have, however, proven without doubt that there is a maximum in the Clausius–Clapeyron equation. This raises the further question of the complete, hypothetical, equilibrium phase diagram, and the possible existence (hypothetical or real) of a truly amorphous reentrant phase, as outlined already in the earlier publication [2,3] and detailed further in the near future [4].

The measured T_m at 550 MPa, at the limit of our HP-DSC, but nevertheless well measurable, indicates another increase in melting temperature at even higher pressures. The reason for this increase is the appearance of the new hexagonal polymorph, as will be discussed below.

4.3. Heat of fusion and crystallinity

The equilibrium value of the heat of fusion of P4MP1 was originally established for the ATHAS data bank from the Clausius–Clapeyron equation at atmospheric pressure and literature data by diluent experiments to be 9.96 kJ mol^{-1} (118 J g^{-1}) [8,21]. Other literature values based on the Clausius–Clapeyron equation alone led to a much lower value due to a smaller ΔV_f ($\Delta H_f = 5.2$ kJ mol^{-1}, 62 J g^{-1}) [22]. From the former data a crystallinity of 34% results, as is indicated in Section 2. From the latter, the crystallinity would be 65%. Only the larger heat of fusion results, however, in an entropy of fusion that agrees with the series of vinyl polymers [16]. Similarly, most helical polymers do not reach crystallinities as one would calculate from the low heat of fusion. Published X-ray powder patterns could not resolve this dispute, since it was suggested that the amorphous pattern is also concentrated in the diffraction-angle region of the crystalline pattern [21].

The heat of fusion of the tetragonal crystals at elevated pressure seems to decrease with increasing pressure to $\Delta H_f(450) = 0.5$ kJ mol^{-1} at 450 MPa, as is shown in Fig. 8. Assuming that the heat of fusion, at least initially, is a pressure independent quantity, we may calculate the change in degree of crystallinity with pressure. Under these conditions, the overall degree of crystallinity

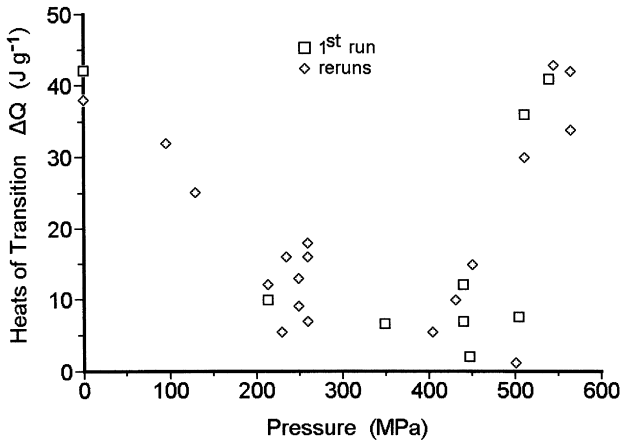

Fig. 8. Measured heats of fusion as a function of pressure.

decreases to as little as 1/7th of the atmospheric pressure value with increasing pressure.

From the HP-DSC results alone, however, it is not possible to conclusively state that the decrease in enthalpy with increasing pressure seen in Fig. 8 is due to a decrease in overall crystallinity, there should also be some pressure dependence of the enthalpy and entropy of fusion. Speculating that the high-pressure melt is still random, one should maintain the conformational entropy of fusion which is usually about 75% of the total ΔS_f. This value of 75% was estimated from over 20 flexible macromolecules, including P4MP1, by comparing the computed conformational entropy with measured entropies of fusion, extrapolated to 100% crystallinity [16]. Assuming further, that at the maximum of T_m as a function of pressure, the volume contribution to the heat of fusion is zero, as derived from the Clausius–Clapeyron equation, one finds from Figs. 7 and 8 that at about 150 MPa the entropy of fusion should be about 60% of its atmospheric pressure value if there were no change in crystallinity. On the basis of this discussion, one would suggest that both, sizeable decreases in crystallinity and entropy of fusion occur.

The possibility of some thermal degradation cannot be fully ignored in this discussion. This could also have an influence on the decrease in overall crystallinity at the elevated temperature and pressure. To have an estimation of the possible influence of thermal degradation on overall crystallinity of the sample, we reran some samples after high-pressure treatment in a standard DSC at atmospheric pressure. At best, we found a 10–20% lower heat of melting than was measured with the as-received material for several, but not all samples. This discrepancy is similar to the dispersion of the heats of fusion at different pressures summarized in Fig. 8. Therefore, the change in the measured heats of fusion with pressure must be attributed to pressure rather than thermal degradation which may arise with the number of reruns along path 3.

To conclude the crystallinity discussion, it should be mentioned, that no glass transition step could be seen in DSC curves, neither at ambient pressure in the normal DSC, nor at other pressures in the HP-DSC, with the exception of one single point at 550 MPa. This means that the noncrystalline phase should be over wide temperature ranges in the rigid amorphous state [23], as is a frequent occurrence in helical and somewhat stiffer macromolecules.

4.4. Hexagonal P4MP1

Of particular interest is the newly discovered hexagonal phase [2–4]. A high pressure phase that could be analyzed as a metastable crystal at room temperature and atmospheric pressure with a similar X-ray pattern like ours, but with an unknown structure was reported earlier by isothermal heat treatment of the tetragonal phase at 200–270°C at 450 MPa, followed by cooling and pressure release [24]. As a metastable phase at room temperature and atmospheric pressure, a crystallographic structure determination could be undertaken recently [4]. The crystals have hexagonal symmetry with unit cell dimensions at the room temperature and atmospheric pressure of $a = b = 16.88$ Å, $c = 6.30$ Å, and angles $\alpha = \beta = 90°$ and $\gamma = 60$. The length of c is consistent with eight trigonal vinyl polymers with $2^*3/1$ helices that have been reviewed earlier [1]. Compared to poly(3-cyclohexylpropene) with a three carbon-atom larger side chain, the similarity is obvious $a = b = 19.12$ Å $c = 6.33$ Å, $\alpha = \beta = 90°$ and $\gamma = 60°$). The calculated crystal density of the hexagonal phase of P4MP1 (at atmospheric pressure) is 0.826 Mg m^{-3}, higher than that of the loosely packed tetragonal P4MP1 (0.822 Mg m^{-3}) [1], but still somewhat lower than the amorphous density at room temperature (0.838 Mg m^{-3}) [16]. A more detailed structural investigation is in progress elsewhere [25].

4.5. Disordered high-pressure P4MP1

Below the glass transition temperature, along the isothermal path 1 of Fig. 1, X-ray diffraction and Raman spectroscopy could show the loss of the tetragonal crystal structure and a transformation to a disordered phase, a condis glass, as summarized in Section 1 [2–4]. Fig. 3 shows the calorimetric evidence for this change. The transition appears reproducibly at about 200 MPa and is exothermic in nature (■ in Figs. 1, 2, and 7). The molar heat of transition is only about -70 J mol^{-1} (-0.9 J g^{-1}). Assuming the transition was reversible and is only connected to the crystalline phase, this would give rise to a decrease in molar entropy for a 100% crystalline sample of -0.7 J K^{-1} mol^{-1}, a value that cannot be linked to complete disordering since this would require a large and positive entropy change. The only solution is an increase in entropy due to disordering which is overcompensated by a decrease in entropy due to densification. These competing entropy changes should be compared to the entropy of fusion at atmospheric pressure ($+9.96$ J K^{-1} mol^{-1}). Of this amount about 75% is due to conformational disordering and the rest can account for the cohesive energy and other contributions as mentioned above

[16]. These orders of magnitude in entropy contribution make it impossible that the observed small entropy change can be the difference between two large numbers. Furthermore, it must be remembered that this transformation occurs below T_g, i.e. the large-amplitude, cooperative conformational motion in the amorphous defects, as well as at the interface to the crystals is frozen, and chain reorientation and translation are similarly impossible. The observation must, thus, be described as local disordering, keeping much of the conformational, orientational, and translational correlation, a conclusion that agrees also with the Raman data [4].

The subsequent experiments of Okumura et al. [9], display in their published X-ray diffraction patterns the same features of pressure induced disordering. With the above, more detailed definitions of disordering, we must assume that the "disorder of the first kind" that was suggested and the "amorphization" are referring to the same effect with differences being caused by varying degrees of shear stress, crystallization, and sample origin.

Extending the estimate of entropy contributions somewhat further, one can assume that the correction of the packing fraction by 2%, as it exists between crystal and amorphous phase at atmospheric pressure, could yield under equilibrium conditions at 200 MPa a change in heat content of about $-1.7\ \mathrm{J\,g^{-1}}$ (assuming 34% crystallinity, and a crystal density 0.822 $\mathrm{Mg\,m^{-3}}$). Taking the measured heat effect of $-0.9\ \mathrm{J\,g^{-1}}$ at face value, this can compensate an endotherm of $0.8\ \mathrm{J\,g^{-1}}$ or a change in conformational entropy of $+0.65\ \mathrm{J\,K^{-1}\,mol^{-1}}$ at 300 K and corrected to 100% crystallinity. This small increase in entropy must be compared to an expected increase in entropy on conformational disordering about a single backbone bond of $10-12\ \mathrm{J\,K^{-1}\,mol^{-1}}$ [16]. Even arguing a substantial decrease in entropy of fusion with pressure, as discussed above, there is only a small calorimetrically noticeable disorder introduced when compared to melting.

There are, however, many cases were nanometer-size crystals, which give no sharp X-ray diffractogram, still produce a sizable entropy of fusion [16]. In addition, there are other cases of polymer samples with similarly "amorphous" X-ray diffraction patterns, but with a semicrystalline heat of fusion. Particularly well known is quenched polypropylene which had been interpreted as a smectic liquid-crystalline material on the strength of the X-ray evidence [26], but is today better termed a CD glass with a frozen-in structure of conformational defects (helix reversals) [7]. On heating through its glass transition it shows an exotherm of only 17% of the heat of fusion observed on final fusion.

The Raman spectroscopic measurements [4] along path 1 of the p–T phase diagram in Fig. 1 seem to show that not only are backbone bonds affected by the transition, but also the packing of the side-chains. The very small entropy changes and the Raman results focus attention to the side groups as the major sites of change and source of disorder. We propose on this evidence a similar, but reverse process as in heating of polypropylene for the isothermal transition in P4MP1 along path 1 in Fig. 1. The larger compressibility of the less dense crystals generates an increasing strain between the phases, until a collapse into a mosaic of small crystals with limited conformational disorder yields a more closely packed, metastable structure. The detailed scale and nature of the disordered structure are still unknown, but the missing crystalline X-ray diffraction peaks limits the order to the nanometer scale, while the calorimetry can only account for a limited gain in entropy, compensated by the strain reduction by the crystal break-up. In this way, most of the heat of fusion (and crystallinity) at atmospheric pressure can be retained. Since cooperative large-amplitude mobility does not exist below T_g, the overall transition seems partially mechanical in nature. Overall, it may be possible to call this state a CD glass, although the nature of the limited conformational disorder is not fully established and may involve side-chain disorder, as suggested by Raman spectroscopy [4]. In more detail, the sample may be a microcrystalline, defect crystal aggregate, embedded in glassy, amorphous defects. Of particular interest are the processes that occur on exceeding the glass transition of the amorphous defects, as will be described in the next section.

A final question concerns the observed reversing of the disorder on pressure release. No measurable endotherm was observed, as would be required for a thermodynamically reversible process. Below the glass transition, one probably could not expect such a process. Making the phase area indicated in Fig. 7 by the dotted line, metastable. One may, however speculate that the phase-line 2 in the equilibrium-diagram of Fig. 6 may in some way connect to this dotted line. In this case, the disordering would be an equilibrium phase transition of the tetragonal crystals trying to reach the hexagonal symmetry, but frustrated by the surrounding amorphous glass, leading to a shattering of the original crystals without gaining the new symmetry.

4.6. Transition to and from the hexagonal phase

The transitions to and from the hexagonal phase are not straightforward. The hexagonal phase can seemingly only be entered on isobaric heating from the disordered phase. Further, once entered, this phase is retained irreversibly on cooling and also on subsequent pressure release. From the equilibrium phase diagram of Fig. 6 one could imagine three other entries into area H, directly by isobaric cooling from the melt, and either isobaric or isothermal paths from and to the tetragonal phase. All of these are, however, hindered. On the other hand, once formed, Fig. 8 shows that the heat of fusion of the hexagonal phase to melt increases conspicuously with pressure, suggesting the development of higher degrees of crystallinity and possibly also a higher heat of fusion. It would be of great interest to study the crystallization and melting of the hexagonal phase above the triple point.

The DSC traces reproduced in Fig. 5 show the entry to

hexagonal symmetry via path 2 (curve a) and path 3 (curve b). Both traces display a small, but clearly identifiable endotherm of 1.5 ± 0.3 J g^{-1}. Normally small endotherms observed on heating could signify a solid–solid transition to high-temperature crystal structures, a minor amount of melting, or going through the glass transition of a densified glass with an enthalpy relaxation [16].

An enthalpy relaxation at the glass transition may be easily of the observed 1–2 J g^{-1} size, but would be heating and cooling rate dependent. Since, however, glass transitions were usually not observed in the calorimetry, we must assume that the glass transition of the semicrystalline material is broad [19]. The enthalpy relaxation would in this case also be hardly visible, as was recently analyzed quantitatively for semicrystalline poly(ethylene terephthalate), using kinetic parameters derived from data gained from temperature-modulated DSC [27]. Furthermore, the glass transition line indicated in Fig. 7, which was derived from Brillouin scattering, is somewhat lower than the endotherms. This would make it more likely that the endotherm is connected with processes of the crystals that were arrested by the amorphous defects. Other examples of such behavior are the well-known exothermic cold crystallizations, possible when quenched polymers are heated above their glass transitions.

Melting and crystallization of crystals has a much larger enthalpy of transition than in path 2 at ≈ 100°C, as can be seen from Fig. 8. In addition, the X-ray results [4] indicate that the heating paths 1 and 3 are changing from disordered (or nano-size, defect crystals) to better crystals, the newly recognized hexagonal phase H (see Figs. 1, 2, 6 and 7). If an increase in order, however, is the only process happening, it must be exothermic. This leaves two other possibilities. Firstly, some of the smallest crystals melt with an endotherm and do not recrystallize, while the others perfect or recrystallize to the hexagonal structure with an exotherm, giving the overall endotherm. Such a process, however, one should not be able to reverse. It seems unlikely that the metastable, smallest crystals formed by isothermal compression (path 1) can be recreated in similar amounts by isobaric cooling (path 3), as indicated by the heats of transition given in Table 2 (see also Fig. 5).

The second alternative would be a solid–solid transition from the tetragonal to the hexagonal symmetry. Although this interpretation would be the easiest for curve a of Fig. 5, it is untenable for curve b. Once the hexagonal phase is formed, there is no thermodynamic driving force for reversing it back to tetragonal (see Fig. 6). And although disorder is produced on cooling along path 3 of Fig. 1, no tetragonal phase is evident.

Having thus exhausted all obvious possibilities, one must assume that decreasing the temperature along path 3 again breaks up the crystals, now hexagonal, but seemingly in a more gradual process, so that the accompanying heat effect cannot be identified. Assuming the endotherm in Fig. 5 is related to the reverse of the exotherm in Fig. 3, one may suggest on the basis of the Raman data [4], that in the region of the disordered phase in Fig. 7 small, nanophase crystals are present caused by problems of the packing of the side groups. If this were true, the remaining interesting question is if this disordered and metastable phase were not arrested by the glass transition, would it drift into a phase related to the high temperature melt? This exceedingly interesting question is further analyzed in another publication [4].

4.7. Metastable crystals

A further significant feature of the phase diagram of Fig. 7 is a number of endothermic prepeaks marked as △ (see also Table 1). The very small prepeaks found in some isobaric heating reruns along paths 3 have a heat of transition of less than 80 J mol^{-1} (0.97 J g^{-1}) with a $\Delta S < 0.6$ J K^{-1} mol^{-1} recalculated for 100% crystallinity. With the help of X-ray data [1,4] which have recently been extended [28], one can assign these systematic, but not always reproducible peaks to the phase transitions of the hexagonal to the tetragonal phase. Fig. 7 shows that the region of these transitions is rather broad, the lower line is assumed to be related to line #2 of the equilibrium phase diagram in Fig. 6. The upper endotherms mark the high-temperature limit of observed metastable hexagonal crystals. Between the dotted and solid line of Fig. 7 X-ray diffraction shows the presence of both, tetragonal and hexagonal crystals. It is known that the melting point of the metastable hexagonal phase at ambient pressure is 127°C, supporting the atmospheric pressure point on the dotted line drawn in Fig. 7 [4,29].

The intersection of line 2 with the line 1 in Fig. 6 corresponds to the T–H–L triple-point, postulated earlier [2–4]. Again, confirming this previous attribution by X-ray diffraction. It also shows how the new hexagonal crystal phase intervenes between liquid and disordered phase regions.

5. Conclusions

A schematic equilibrium phase diagram of P4MP1 is shown in Fig. 6, based on the more detailed nonequilibrium phase diagram of Fig. 7. The equilibrium phase diagram excludes all metastable and glassy phase areas.

The Clausius–Clapeyron equation describes the melting of the tetragonal phase, showing a rare maximum due to an inversion of the volume change on fusion. Moreover, heat of fusion and crystallinity decreases with increasing pressure, suggesting the possibility of a re-entrance of two widely separated disordered phases along the temperature axis of the phase diagram, as is detailed elsewhere [2–4]. Before the entropy of fusion approaches zero, however, another reversal in the change of heat of fusion with pressure is observed (Fig. 8) due to the intervention of a hexagonal polymorph with higher density than the tetragonal phase (see Fig. 6), giving rise to the triple point in the equilibrium phase diagram of Fig. 6.

Proceeding below the glass transition along path 1 in

Fig. 1, an exotherm marks the isothermal transition from the semicrystalline, tetragonal phase to a nonequilibrium, disordered, but metastable phase, as was reported earlier based on X-ray diffraction [2,3]. Its exothermic nature suggests that the overall entropy for the disordered phase is lower than that of the semicrystalline phase. Of several interpretations it seems most likely that the state is a semicrystalline CD glass, in more detail, a microcrystalline, defect aggregate of nanometer-size crystals, embedded in glassy, amorphous defects.

On heating along path 2, an endothermic transition indicates a transition of the disordered phase to a hexagonal, semicrystalline state. The transition is observed about 20°C above the glass transition temperature drawn in Fig. 7. Transitions that require minimal reorientations are normally anticipated during cold crystallization, but in the present case the transition is overall endothermic. Since this transition is repeatable by cooling and reheating along paths 3, it is likely that among several possibilities the endotherm is related to the reverse of the exotherm seen along path 1, and one may suggest on the basis of Raman data [4] that in the region of the disordered phase in Fig. 7 small, nanophase crystals are present, caused by problems of the packing of the side groups arising either by compression of the tetragonal phase (path 1) or by cooling along path 3.

The calorimetric observations, supported by X-ray data [4], suggest a metastable region for the hexagonal phase in the thermodynamically stable regime for the tetragonal phase (see Fig. 7).

Acknowledgements

Special thanks go to Drs Blankenhorn and Schawe for measurements contributed to this work. Major financial support came from the German DFG (SFB 239). One of us was supported during the discussion and rewriting of the paper by the Division of Materials Research, National Science Foundation, Polymers Program, Grant #DMR-9703692 and the Division of Materials Sciences, Office of Basic Energy Sciences, US Department of Energy at Oak Ridge National Laboratory, managed by Lockheed Martin Energy Research Corp. for the US Department of Energy, under contract number DE-AC05-96OR22464.

References

[1] Wunderlich B. Crystal structure, morphology, defects, Macromolecular Physics, vol. 1. New York: Academic Press, 1973.
[2] Rastogi S, Newman M, Keller A. Nature 1991;353:55.
[3] Rastogi S, Newman M, Keller A. J Polym Sci, Part B: Polym Phys 1993;31:125.
[4] Rastogi S, Höhne GWH, Keller A. Submitted for publication.
[5] Mishima O, Clavert LD, Whalley E. Nature 1984;310:393.
[6] Mishima O, Clavert LD, Whalley E. Nature 1985;314:76.
[7] Wunderlich B, Möller M, Grebowicz J, Baur H. Conformational motion and disorder in low and high molecular mass crystals, Advances in polymer science, vol. 87. Berlin: Springer, 1988.
[8] Jain AK, Wunderlich B. JPolym Sci, Polym Phys Ed 1977;15:2271.
[9] Okumura S, Miyaji H, Izumi K, Toda A, Miyamoto Y. Polymer 1996;11:2285.
[10] Blankenhorn K, Höhne GWH. Thermochim Acta 1991;187:219.
[11] Sarge SM, Hemminger W, Gmelin E, Höhne GWH, Cammenga HK, Eysel W. J Thermal Anal 1997;49:1125.
[12] Höhne GWH, Dollhopf W, Blankenhorn K, Mayr PU. Thermochim Acta 1996;273:17.
[13] McDaniel ML, Babb Jr. SE, Scott GJ. J Chem Phys 1962;37:822.
[14] Müller J, Pietralla M. University Ulm, Germany, private communication.
[15] Wunderlich B. Crystal nucleation, growth, annealing, Macromolecular physics, vol. 2. New York: Academic Press, 1976.
[16] Wunderlich B. Crystal melting, Macromolecular physics, vol. 3. New York: Academic Press, 1980 (For updates and coverage of thermal analysis see also: Thermal analysis, Academic Press, Boston, 1990, and Thermal analysis of materials; a computer-assisted lecture course of 36 lectures on over 3,000 screens, published on the World Wide Web (URL: http://web.utk.edu/~athas/courses/tham99.html), downloadable including presentation software, 1998/99).
[17] Sumpter BG, Noid DW, Liang GL, Wunderlich B. Adv Polym Sci 1994;116:27.
[18] Wunderlich B, Grebowicz J. Adv Polym Sci 1984;60(61):1.
[19] Wunderlich B. Pure Appl Chem 1995;67:1919.
[20] Zoller P. J Appl Polym Sci 1977;21:3129.
[21] Karasz FE, Bair HE. O'Reilly. Polymer 1967;8:547.
[22] Zoller P, Starkweather Jr HW, Jones GA. J Polym Sci, Part B: Polym Phys 1986;24:1451.
[23] Suzuki H, Grebowicz J, Wunderlich B. Bri Polym J 1985;17:1.
[24] Hasegawa R, Tanabe Y, Kobayashi M, Tadokoro H, Sawaoka A, Kawai N. J Polym Sci, Part A-2 1970;8:1073.
[25] Lotz B. Private communication.
[26] Natta G, Peraldo M, Corradini P. Rend Accad Naz Lincei 1959;24:14.
[27] Okazaki I, Wunderlich B. J Polym Sci, Part B: Polym Phys 1996;34:2941.
[28] Deutsch B, Müller J. University of Ulm, Germany, private communication.
[29] Phase II of Takayanagi M, Kawasaki N. J Macromol Sci -Phys Part B 1967;1:741.